Impact of isospin breaking on the distribution of transition probabilities

C. I. Barbosa, T. Guhr, and H. L. Harney
Max-Planck-Institut für Kernphysik, Postfach 103980, 69029 Heidelberg, Germany
(Received 22 November 1999)

In the present paper we investigate the effect of symmetry breaking in the statistical distributions of reduced transition amplitudes and reduced transition probabilities. These quantities are easier to access experimentally than the components of the eigenvectors and were measured by Adams *et al.* [Phys. Lett. B **422**, 13 (1998)] for the electromagnetic transitions in ^{26}Al. We focus on isospin symmetry breaking described by a matrix model where both the Hamiltonian and the electromagnetic operator break the symmetry. The results show that for partial isospin conservation, the statistical distribution of the reduced transition probability can considerably deviate from the Porter-Thomas distribution.

PACS number(s): 05.45.−a, 24.60.Lz, 11.30.Er

I. INTRODUCTION

The spectral fluctuations in a rich variety of different physical systems show, if measured on the scale of the local mean level spacing, very similar features. This high degree of universality makes it possible to describe these fluctuations with random matrices. Random matrix theory (RMT) is a simple, schematic model in which the matrix elements of the Hamiltonian in some basis are replaced with random numbers. Apart from randomness, the only further input are the symmetries and invariances of the system, in particular time reversal invariance. It turns out that this assumption of full ergodicity or ''chaoticity'' leads, in many cases, to a complete and parameter-free description of the spectral fluctuations. Such universal cases are said to be of the Wigner-Dyson type. We refer the reader to the reviews in Refs. [1,2]. Originally, Wigner had developed this approach in nuclear physics where it continues to find new applications.

In recent years, interest has been focused on deviations from the universal, parameter-free Wigner-Dyson fluctuations. The deviations can have different reasons, such as regular effects competing with full chaoticity or the breaking of time-reversal invariance, see Ref. [2]. Here, we wish to discuss deviations attributed to the breaking of isospin symmetry. We recall that symmetries such as isospin or parity are, in contrast to time-reversal invariance, associated with quantum numbers. In the context of spectral fluctuations and RMT, symmetry breaking already received broad interest, see the compilation in Ref. [2]. As early as 1960, Rosenzweig and Porter [3] analyzed atomic spectra by setting up a general random matrix model which describes crossover transitions between different angular momentum coupling schemes. In the late eighties, Mitchell *et al.* [4] measured and analyzed about 100 low-lying states with known values of the isospin quantum number in the nucleus ^{26}Al. In Ref. [5], this was discussed in the framework of a random matrix model which is a special case of the Rosenzweig-Porter model. An estimate for the statistical Coulomb matrix element, i.e., a measure for the degree of isospin breaking, could be obtained. Motivated by similar questions in molecular physics, Leitner and co-workers [6] performed a perturbative calculation of the spectral fluctuations in the random matrix model. More recently, additional data were obtained in two statistically highly significant experiments on the breaking of a point-group symmetry in a resonating quartz block [7], and the coupling of two chaotic microwave billiards [8]. Both cases, although physically very different, are statistically fully equivalent to symmetry breaking in quantum mechanics. Importantly, there is only one parameter entering the random matrix model. It is a unique measure, e.g., for the root-mean-square statistical Coulomb matrix element. This illustrates that the random matrix model is the ideal tool to extract a root-mean-square symmetry-breaking matrix element from the data.

All these studies addressed the *spectral* fluctuation properties. Symmetry breaking, however, will also have an impact on the statistics of the *wave functions* and observables sensitive to them. Recently, Adams, Mitchell, and Shriner [9] collected reduced γ-ray transition probabilities from different experiments on ^{26}Al. As mentioned above, this nucleus had already shown a strong deviation of the *spectral* fluctuations from the universal Wigner-Dyson result due to isospin breaking [4]. The new results [9] show that the distribution of the *transition* probabilities also considerably deviates from the Wigner-Dyson statistics, i.e., from the distribution that corresponds to full, parameter-free ''chaos.'' In the present contribution, we wish to discuss these results. To this end, we extend the random matrix model of Ref. [5] to discuss transition probabilities. Similar investigations were performed simultaneously and independently by Andersen *et al.* [10] for symmetry breaking in acoustic and elastomechanical systems.

This paper is organized as follows. In Sec. II we briefly review the experimental results on the reduced transition probabilities in ^{26}Al collected by Adams, Mitchell, and Shriner [9]. In Sec. III we discuss the random matrix model in the case that no symmetry is present, in particular its predictions for transition probabilities. The random matrix model for isospin breaking is numerically studied in Sec. IV. In Sec. V the numerical simulation is approximated by a qualitative albeit analytical model. The data analysis is performed in Sec. VI. The summary and conclusion are presented in Sec. VII.

II. EXPERIMENTAL RESULTS

Experimental reduced electromagnetic transition strengths between the excited states of the nucleus ^{26}Al have been

collected by Adams, Mitchell, and Shriner, see Ref. [9]. Their data involve levels between the ground state and the excitation energy of 8.067 MeV. In this region, states with isospin $T=0$ and $T=1$ are found and isospin is known to be approximately conserved.

The probability B_{if} of a transition from the initial configuration $|i\rangle$ to the final configuration $|f\rangle$ is the square

$$B_{if}=|W_{if}|^2 \tag{1}$$

of the matrix element

$$W_{if}=\langle f|\mathcal{O}|i\rangle \tag{2}$$

of the relevant transition operator $\mathcal{O}$ in a special basis.

Approximately 180 levels and 1500 electromagnetic transitions are known. The fluctuations of the B_{if} values shall be studied. To this end, their systematic dependence on the quantum numbers of the initial and final states must be removed. This has been done in Ref. [9] in the following way. The states in ^{26}Al have been characterized by their excitation energy E, spin J, parity π, and isospin T. Transitions are characterized by their electromagnetic character X which may be $\mathcal{E}$ or $\mathcal{M}$, their multipolarity L, and a label τ which becomes isoscalar (IS) if $\Delta T=0$ and isovectorial (IV) if $\Delta T=1$. Hence, both the transition operator $\mathcal{O}=\mathcal{O}(XL,\tau)$ and the transition probabilities $B_{if}=B_{if}(XL,\tau)$ are functions of X, L, and τ. We shall, however, not always write all these arguments.

A *transition sequence* is defined as a set of reduced transition probabilities where the initial states have a common assignment J^π, T, the final states have a common assignment $J'^{\pi'}$, T', and the transitions have their three defining characteristics all the same. Thus the reduced transition probabilities $B_{if}=B(E_i,E_f)$ of a given transition sequence can be labeled by the energies E_i and E_f of the initial and final states, respectively. The aforementioned secular variations of the B values were removed by normalizing them to the local average value $\langle B(E_i,E_f)\rangle$ of $B(E_i,E_f)$ so that the statistical variable used further on is

$$y(E_i,E_f)=\frac{B(E_i,E_f)}{\langle B(E_i,E_f)\rangle}. \tag{3}$$

The local average is defined with the help of weighting factors that are Gaussian functions of the excitation energies. In doing so one must, however, remove the systematic dependence of the local level distance D on the excitation energy; i.e., one measures the energy in units of D and works with a dimensionless energy

$$\varepsilon=\frac{E}{D}. \tag{4}$$

The details are given in Ref. [11]. The local average of the B values of a given transition sequence is then

$$\langle B(\varepsilon_i,\varepsilon_f)\rangle=\frac{\sum_{\varepsilon,\varepsilon'} B(\varepsilon,\varepsilon')\ e^{-(\varepsilon_i-\varepsilon)^2/8}e^{-(\varepsilon_f-\varepsilon')^2/8}}{\sum_{\varepsilon,\varepsilon'} e^{-(\varepsilon_i-\varepsilon)^2/8}e^{-(\varepsilon_f-\varepsilon')^2/8}}. \tag{5}$$

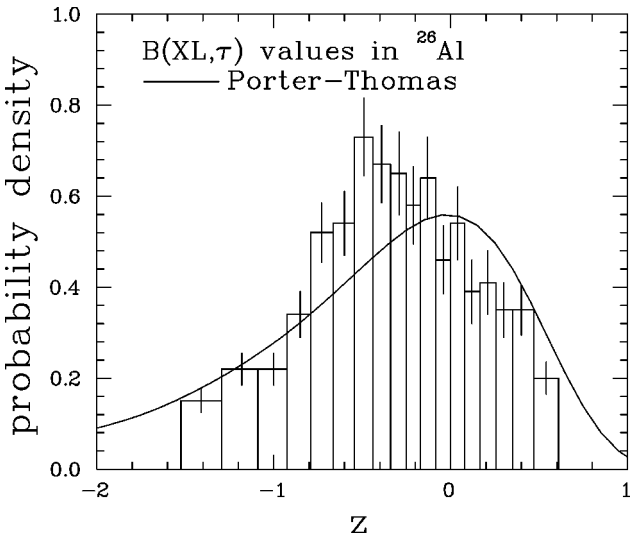

FIG. 1. The distribution of experimental reduced transition probabilities $B(XL,\tau)$ in ^{26}Al from Ref. [9]. The quantity B has been transformed to the logarithmic variable z of Eq. (6). The curve labeled Porter-Thomas is the distribution (9).

The fact that the variance of the Gaussian functions has been chosen equal to 4 is discussed in Ref. [11].

It is clear that the definition of the quantities $y=y(E_i,E_f)$ requires the necessary spectroscopic information for the relevant states in ^{26}Al. Furthermore, the local averages D and $\langle B(E_i,E_f)\rangle$ require that there is a minimum number of members in the sequences from which these averages are derived. These restrictions have finally led in Ref. [9] to an ensemble of 873 values of y.

The authors of Refs. [9,11] have found it convenient to transform y to the logarithmic variable

$$z=\log_{10} y. \tag{6}$$

The experimental distribution of z is given by the histogram on Fig. 1. Although the widths Δz_k of the bins $k=1,\ldots,18$ in Fig. 1 vary, the ordinate is the probability density with respect to z: The height p_k of the kth bin is

$$p_k\sim\frac{N_k}{\Delta z_k}, \tag{7}$$

where N_k is the number of cases falling into the kth bin.

Since the states $|i\rangle$ and $|f\rangle$ are believed to be ''very complicated,'' it is natural to assume that the matrix elements (2) have a Gaussian distribution; see the discussion in Sec. III B. This entails that y has a Porter-Thomas distribution with unit average value, i.e.,

$$P(y)=\frac{1}{\sqrt{2\pi}}\frac{\exp(-y/2)}{\sqrt{y}}. \tag{8}$$

Transforming this to the variable z yields

$$P(z)=\frac{\ln(10)}{\sqrt{2\pi}}10^{z/2}\exp(-10^z/2). \tag{9}$$

A comment on the notation is in order: For every probability density we shall use the symbol P. The fact that we deal with different functions will be clearly indicated by the argument of the probability density in question.

The distribution (9) is given in Fig. 1 for comparison with the data. The distribution (9) is normalized to unity; the histogram of the data, however, has been normalized to

$$\sum_{k=1}^{18} p_k \Delta z_k = 0.83 \tag{10}$$

by the authors of Ref. [9]. This is motivated [12] by the fact that $\int dz\, P(z)$ over the range of the data amounts to 0.83 and approximately takes care of the upper and lower detection thresholds.

The point of Ref. [9] is the shift of the experimental distribution with respect to the Porter-Thomas distribution $P(z)$. The maximum of the histogram occurs around $z=-0.5$. The maximum of $P(z)$ occurs at $z=0$. The authors of Ref. [9] have conjectured that the discrepancy between the experimental data and the Porter-Thomas distribution may be a consequence of isospin breaking in ^{26}Al. The following sections of the present paper focus on this conjecture. In the next section, a random matrix model of isospin violation—and more generally of symmetry breaking—is presented.

III. RANDOM MATRIX MODEL — THE CASE OF NO SYMMETRY

In Sec. III A, we briefly review the distributions of wave functions and widths for the standard Wigner-Dyson case in which no symmetry is present. A more detailed presentation with further references can be found in Ref. [2]. In Sec. III B, we work out the distribution of the transition matrix elements for the same case.

A. Wave functions and decay amplitudes

If the system is invariant under time reversal, the wave functions can be chosen real and the $N\times N$ random matrix H modeling the Hamiltonian is real and symmetric. The matrix elements are Gaussian distributed random numbers and H is said to be in the Gaussian orthogonal ensemble (GOE). In the physically relevant limit of infinitely many states, $N\rightarrow\infty$, the fluctuation properties are of Wigner-Dyson type. A wave function is modeled by an eigenvector u_i, $i=1,\ldots,N$ of H, i.e., we have $Hu_i=E_iu_i$, where E_i is the eigenenergy.

We are interested in the probability density $P(a)$ of finding the value a with $-1\leqslant a\leqslant +1$ for a component u_{im} of the eigenvector u_i. For finite N one finds

$$P_N(a)=\frac{\Gamma(N/2)}{\sqrt{\pi}\,\Gamma((N-1)/2)}(1-a^2)^{(N-3)/2}. \tag{11}$$

The second moment of this distribution is $\overline{a^2}=1/N$. For a large number of levels one obtains a Gaussian with variance $1/N$, i.e.,

$$P_N(a)=\sqrt{\frac{N}{2\pi}}\exp\left(-\frac{N}{2}a^2\right)=G(a,N^{-1/2}). \tag{12}$$

Here, we have introduced the notation $G(a,\sigma)$ for a Gaussian with variance σ^2.

The wave functions are rarely accessible in an experiment. However, other observables, such as scattering matrix elements or partial widths, sensitively depend on them. Consider the scattering from a state i with wave function u_i into a channel c with channel wave function χ_c. The corresponding reduced partial width amplitude γ_{ic} can be written as

$$\gamma_{ic}=\sum_{m=1}^{N} u_{im}J_{mc}, \tag{13}$$

where J_{mc} is the overlap integral between the mth canonical basis vector and χ_c. Again, the probability density can be worked out

$$P(\gamma)=\frac{\Gamma(N/2)}{(\pi N\overline{\gamma^2})^{1/2}\Gamma((N-1)/2)}\left(1-\frac{\gamma^2}{N\overline{\gamma^2}}\right)^{(N-3)/2}, \tag{14}$$

where we suppress the indices i and c. The second moment reads $\overline{\gamma^2}=\overline{\gamma_{ic}^2}=N^{-1}\Sigma_{m=1}^{N}J_{mc}^2$. We notice that the functional form of this distribution agrees with that of Eq. (11). Thus, in the limit of large N, one again finds a Gaussian. Usually, one introduces the partial width $\Gamma=\gamma^2$ which can be measured. The relative partial width $y=\Gamma/\overline{\Gamma}$ with $\overline{\Gamma}=\overline{\gamma^2}$ is distributed according to the Porter-Thomas law (8).

We notice that the Porter-Thomas law or, equivalently, the Gaussian for the partial width amplitudes γ, results from a large N expansion of the distribution (14). Alternatively, one may derive these large N results by using the central limit theorem: The partial width amplitudes are, according to Eq. (13), given as a linear combination of N components u_{im}. If, as assumed in Eq. (14), all these components are independently distributed, the distribution of the partial width amplitudes approaches a Gaussian for large N. This line of arguing does not use the fact that the distribution of every single component u_{im} is Gaussian for large N. It would apply for any smooth distribution of u_{im}, provided it does not sensitively depend on N. This subtle point will be important in Sec. IV A.

B. Transition matrix elements

The results compiled in Sec. III A apply to the partial widths and to their amplitudes. However, in the experiments on ^{26}Al, electromagnetic transition probabilities $B_{if}(XL)$ were measured which are squares of transition matrix elements according to Eqs. (1) and (2). In Refs. [13,14] it is argued that the distribution of the transition matrix elements W_{if} is, once more, of the form (11) and (14). In the present section, however, we give a derivation, valid for large N, which is well suited for the discussion of isospin breaking in Sec. IV.

In our model the initial state $|i\rangle$ and the final state $|f\rangle$ are represented by the eigenvectors u_i and u_f, respectively. The electromagnetic transition operator $\mathcal{O}(XL)$ is modeled by one fixed random matrix. It is not necessary to consider an ensemble of such operators. Thus, the transition matrix elements $W_{if}(XL)$ are given by

$$W_{if}(XL)=u_f^T\,\mathcal{O}(XL)\,u_i=\sum_{nm}\,u_{fn}\mathcal{O}_{nm}(XL)u_{im}. \quad (15)$$

The transition probabilities read $B_{if}(XL)=|W_{if}(XL)|^2$. Although these quantities differ from the partial widths and their amplitudes, it is intuitively obvious that, for large N, the $W_{if}(XL)$ are Gaussian distributed and that the $B_{if}(XL)$ obey a Porter-Thomas law: Since we always consider $i\neq f$, the $W_{if}(XL)$ are linear combinations of (products of two) independent variables and, therefore, the central limit theorem applies.

More precisely, the distribution of the matrix elements W_{if} reads

$$P(W_{if})=\int d[u_i]P(u_i)\int d[u_f]P(u_f)\,\delta(W_{if}-u_f^T\mathcal{O}u_i), \quad (16)$$

where we suppress the argument XL of W_{if} and $\mathcal{O}$. Since we may assume that N is large, the distributions of the components u_{im} and u_{fm} take the form

$$P(u)=\prod_{m=1}^{N}\sqrt{\frac{N}{2\pi}}\exp\left(-\frac{N}{2}u_m^2\right)=\left(\sqrt{\frac{N}{2\pi}}\right)^N\exp\left(-\frac{N}{2}u^Tu\right) \quad (17)$$

with u standing for either u_i or u_f. We notice that the integration domain for each of the eigenvector components is the interval $[-1,+1]$. However, since we consider the large N limit, the distributions (17) are so sharply peaked at the origin that we may extend the domain of integration to the entire real axis. Using the Fourier transform of the δ function in Eq. (16) we have

$$P(W_{if})=\frac{1}{2\pi}\int_{-\infty}^{+\infty}dt\,\exp(itW_{if})R(t,\mathcal{O}). \quad (18)$$

The Gaussian integrals absorbed in $R(t,\mathcal{O})$ can be done easily,

$$\begin{aligned}R(t,\mathcal{O})&=\left(\sqrt{\frac{N}{2\pi}}\right)^{2N}\int d[u_i]\int d[u_f]\\&\quad\times\exp\left(-\frac{N}{2}[u_i^T\;\;u_f^T]\begin{bmatrix}\mathbb{1}_N & it\mathcal{O}/N\\ it\mathcal{O}/N & \mathbb{1}_N\end{bmatrix}\begin{bmatrix}u_i\\u_f\end{bmatrix}\right)\\&=\det{}^{-1/2}(\mathbb{1}_N+t^2\mathcal{O}^2/N^2)\\&=\exp\left[-\frac{1}{2}\,\mathrm{tr}\ln(\mathbb{1}_N+t^2\mathcal{O}^2/N^2)\right]. \quad (19)\end{aligned}$$

We are interested in large N. This allows us to expand the logarithm and to keep only the first term which is $t^2\mathcal{O}^2/N^2$. Thus we have for large N,

$$R(t,\mathcal{O})=\exp\left(-\frac{\overline{\mathcal{O}^2}}{2}t^2\right), \quad (20)$$

where the second moment of the operator is defined by

$$\overline{\mathcal{O}^2}=\frac{1}{N^2}\,\mathrm{tr}\,\mathcal{O}^2. \quad (21)$$

We assume that the matrix elements $\mathcal{O}_{nm}(XL)$ do not depend on N. Hence, collecting everything, the Fourier transform in Eq. (18) yields

$$P(W_{if})=G(W_{if},\overline{\mathcal{O}^2}^{1/2}), \quad (22)$$

which is the expected result.

IV. RANDOM MATRIX MODEL — THE CASE OF ISOSPIN BREAKING

In Sec. IV A, the model is set up for the case that isospin is partially conserved. In Sec. IV B, numerical simulations are described. Note that we speak of isospin breaking because we have in mind the experiment of Sec. II. The model, however, applies to any other quantum number that is partially conserved.

A. Definition of the model

We consider two isospin values $T=0$ and $T=1$. If isospin were fully conserved, the Hamiltonian H would be block diagonal. The Coulomb interaction, however, destroys this symmetry. In Ref. [5], this was modeled by using random matrices of the form

$$H=\begin{bmatrix}H(0) & 0\\ 0 & H(1)\end{bmatrix}+\alpha\begin{bmatrix}0 & H_C\\ H_C^T & 0\end{bmatrix}, \quad (23)$$

where $H(j),\ j=0,1$ are independent GOE matrices with dimension N_j. The total level number is $N=N_0+N_1$. The $N_0\times N_1$ matrix H_C accounts for the Coulomb interaction. It is real without further symmetries and has Gaussian distributed entries. In this model the parameter α is proportional to the root-mean-square Coulomb matrix element. Since $H(j)$ and H_C have positive and negative entries with equal weight, all observables can only depend on the modulus of α, but not on its sign. Thus, in the sequel, we restrict ourselves to $\alpha\geqslant 0$. We recall that the *spectral* fluctuations are measured on the scale of the local mean level spacing D. Thus, the relevant parameter governing the spectral fluctuations is

$$\lambda=\alpha/D. \quad (24)$$

For $\alpha=0$ we have a noninteracting superposition of two independent GOE's. In this case, the distribution of the eigenvector components of the *full* matrix H, i.e., including the many exact zeros, is given by

$$P_{N_0N_1}(a,0)=g_0^2P_{N_0}(a)+g_1^2P_{N_1}(a)+2g_0g_1\delta(a), \quad (25)$$

where we have introduced the fractional level numbers

$$g_0=N_0/N \quad \text{and} \quad g_1=N_1/N. \quad (26)$$

The distributions $P_{N_j}(a),\ j=0,1$ have to be taken as either Eq. (11) or Eq. (12). Obviously, the total distribution $P_{N_0N_1}(a,0)$ is properly normalized.

As discussed in Ref. [5], the variances of the distributions for the matrix elements are chosen in such a way that the spectra of $H(0)$ and $H(1)$ have the same length and that H becomes a full $N\times N$ GOE matrix [15] for $\alpha=1$ if $N_0=N_1$. This also means that

$$P_{N/2,N/2}(a,1)=P_N(a). \tag{27}$$

For $\alpha=1$ but $N_0\neq N_1$ there are some deviations from the pure GOE results.

For arbitrary α, the distribution $P_{N_0N_1}(a,\alpha)$ is not known analytically. A qualitative model is presented in Sec. V [see Eq. (37)].

The transition matrix elements $W_{if}(XL)$ and the corresponding transition probabilities $B_{if}(XL)$ depend not only on the eigenstates u_i of H, but also on the transition operator $\mathcal{O}(XL)$. Since the latter contains the effective charges or the magnetic g factors of proton and neutron, it causes isospin breaking in addition to the isospin breaking built into Eq. (23). Thus, in the same isospin basis that was used in Eq. (23), we may model the transition operator by a matrix of the form

$$\mathcal{O}=\beta_I\begin{bmatrix}\mathcal{O}(0) & 0\\ 0 & \mathcal{O}(1)\end{bmatrix}+\beta_C\begin{bmatrix}0 & \mathcal{O}_C\\ \mathcal{O}_C^T & 0\end{bmatrix}. \tag{28}$$

Here, each of the matrices $\mathcal{O}(j)$, $\mathcal{O}_C$ will be modeled by one fixed random matrix—as described in Sec. IV B. For later convenience, $\mathcal{O}$ has been written as a function of the two parameters β_I and β_C. However, only the ratio

$$\beta=\beta_C/\beta_I \tag{29}$$

is important since the total strength of $\mathcal{O}$ drops out of the observable y of Eq. (3). For $\beta=0$, configurations with different isospin values are not mixed by $\mathcal{O}$ while for $\beta=1$ the mixing is maximal. For $\beta\to\infty$ the operator $\mathcal{O}$ couples configurations with different isospin only.

We are interested in the distribution of the $W_{if}(XL)$ and the $B_{if}(XL)$. According to the discussion in the previous Sec. III, one is tempted to argue as follows: Since Eq. (15) is general and also holds in the presence of conserved or broken isospin, the transition matrix elements $W_{if}(XL)$ are always a linear combination of products of independently distributed sets of variables u_{im} and u_{fn}. Thus, the central limit theorem should apply and we should obtain a Gaussian distribution for the $W_{if}(XL)$. This should even be true for any smooth distribution for the wave-function components u_{im} and u_{fn}. In other words, the specific form of these latter distributions, which are nontrivial functions of the mixing parameter α, is not important and we would always expect a Gaussian distribution for the transition matrix elements $W_{if}(XL)$. However, this reasoning is incorrect, because it does not make use of a specific basis. In other words: The result of this reasoning is an orthogonally invariant distribution. Within the random matrix model (23) one sees that this cannot be true. The statistical properties of the Hamiltonian H are not orthogonally invariant—except for the special case of no isospin symmetry at all. One sees the lack of orthogonal invariance very clearly in the distribution (25) of the eigenvector components in the case $\alpha=0$: The δ distribution will appear only if the basis vectors have well-defined isospin. In general, the wave-function components are functions of α. These functions parametrically depend on N. This N dependence competes with a large N expansion needed in the derivation of the central limit theorem, whose premises are therefore violated. We illustrate this in Sec. IV B by numerical examples.

B. Numerical simulation

The distributions of the reduced transition amplitudes and reduced transition probabilities were numerically investigated. To this end, random Hamiltonians with the structure of Eq. (23) have been constructed. The dimensions N_0 and N_1 were chosen to be 100 so that H has the dimension $N=200$. The elements of $H(j)$, $j=0,1$, were selected by a generator of Gaussian random numbers such that the second moments were

$$\begin{aligned}H_{\mu\nu}(0)H_{\mu'\nu'}(0)&=\delta_{\mu\mu'}\delta_{\nu\nu'}+\delta_{\mu\nu'}\delta_{\nu\mu'},\\ H_{mn}(1)H_{m'n'}(1)&=\delta_{mm'}\delta_{nn'}+\delta_{mn'}\delta_{nm'},\\ (H_C)_{\mu m}(H_C)_{\mu' m'}&=\delta_{\mu\mu'}\delta_{mm'}.\end{aligned} \tag{30}$$

This ensures that H is a full GOE matrix for $\alpha=1$. The mean spacing D_j of the eigenvalues of $H(j)$ is then (in the center of the spectrum)

$$D_j=\pi N_j^{-1/2}=0.314. \tag{31}$$

The mean level spacing D of H is

$$D=(D_0^{-1}+D_1^{-1})^{-1}=0.157. \tag{32}$$

This value changes little, when α is varied between 0 and 0.157. This range of values was considered in the present numerical simulations. The parameter λ of Eq. (24) then covers the range of $0\leqslant\lambda\leqslant 1.0$. Ten Hamiltonians were constructed and diagonalized for each value of λ.

The transition operator $\mathcal{O}$ was constructed very much as the Hamiltonians, i.e., its elements were selected by the random number generator. The variances were chosen in complete analogy with Eqs. (30). However, for each value of β, one operator has been generated. The range of $0\leqslant\beta\leqslant 1.0$ was covered.

For given parameters λ, β the transition amplitudes (15) have been calculated with the indices i,f running over the eigenvectors of the ten Hamiltonians. The set of 2×10^5 numbers W_{if} with $i>f$ forms the numerically generated data.

In a first step, we have checked whether these data follow a Gaussian distribution. To this end one can bin the set of W_{if} and compare the histogram to a Gaussian; similarly one can compare the distribution of the variable y of Eq. (3) to the distribution (8) or the distribution of z of Eq. (6) to $P(z)$ given in Eq. (9). In order to make the comparison—as much as possible—independent of the parametrization of the statistical variable, the generalized entropy

$$S=-\int dx\, p(x)\ln\frac{p(x)}{P(x)} \tag{33}$$

TABLE I. Entropy for different values of the parameters β and λ. The parameter α is also shown.

λ	α \ β	0	0.02	0.06	0.1	0.4	1.0
0	0	−1.05	−0.75	−0.53	−0.37	−0.04	−0.0003
0.012	0.002	−0.54	−0.53	−0.40	−0.30	−0.04	−0.0003
0.019	0.003	−0.43	−0.42	−0.34	−0.26	−0.04	−0.0003
0.031	0.005	−0.35	−0.34	−0.29	−0.23	−0.03	−0.0003
0.125	0.02	−0.06	−0.06	−0.06	−0.06	−0.01	−0.0003
1.0	0.16	−0.0006	−0.0006	−0.0006	−0.0004	−0.0004	−0.0004

has been used to express the difference between the distribution p of the data and the ansatz P. This expression is independent of the parametrization x. Since both, p and P, are normalized, S is never positive. It vanishes if and only if $p \equiv P$. The data do not, of course, provide a continuous probability density $p(x)$ but rather a histogram where the kth bin is centered at x_k and contributes the probability $p(x_k)\Delta x_k$. Therefore they provide the approximation

$$S \approx -\sum_k \Delta x_k \, p(x_k) \ln \frac{p(x_k)}{P(x_k)} \tag{34}$$

to expression Eq. (33). To the extent that Eq. (34) is a good approximation to Eq. (33), expression (34) is independent of the parametrization. This holds in the present case to within a few times 10^{-4} due to the large ensemble of numerical data. In Table I, the entropy (34) is given for a few values of β and λ in the range of $0 \leqslant \beta, \ \lambda \leqslant 1$. One finds that the distribution of the data does depend on the parameters λ and β which govern the symmetry breaking. The entropy approaches zero, when β or λ approach unity, i.e., when the symmetry is strongly broken. Hence, in this case the transition amplitudes W_{if} have a Gaussian distribution. This does not hold if β and λ have values much smaller than 1, in which case neither the Hamiltonian (23) nor the operator (28) significantly breaks the symmetry.

Figures 2 and 3 illustrate in which way the distribution of W_{if} deviates from a Gaussian. Consider the case of $\beta = 0 = \lambda$, i.e., the absence of symmetry breaking, displayed in Fig. 2(A). There is no transition between different symmetry classes and therefore about one-half of the matrix elements W_{if} vanishes. This leads to the narrow peak in Fig. 2(A) comprising one bin centered at zero. This peak is superimposed over the distribution of the matrix elements connecting states in one and the same symmetry class. Figure 2(A) thus corresponds to Eq. (25) with $N_0 = N_1$. When the symmetry is completely broken—in Fig. 2(D)—the matrix elements W_{if} have a Gaussian distribution. Intermediate situations are displayed in the parts B and C of Fig. 2.

The intermediate situation is especially well visualized on Fig. 3, where the distributions of Fig. 2 have been transformed to the logarithmic variable

$$z = \log_{10} \frac{W_{if}^2}{\overline{W_{if}^2}}, \tag{35}$$

which was introduced in Eq. (6).

Here, the distribution displays two peaks. One of them, centered at $z = 0$, stems from the matrix elements connecting states within one symmetry class. The other one, centered at negative values of z, is due to the matrix elements connecting states from different symmetry classes. In case of complete symmetry breaking the two peaks merge as in Fig. 3(D). This distribution corresponds to Eq. (9). In the present parametrization the case of no symmetry breaking [Fig. 3(A)]

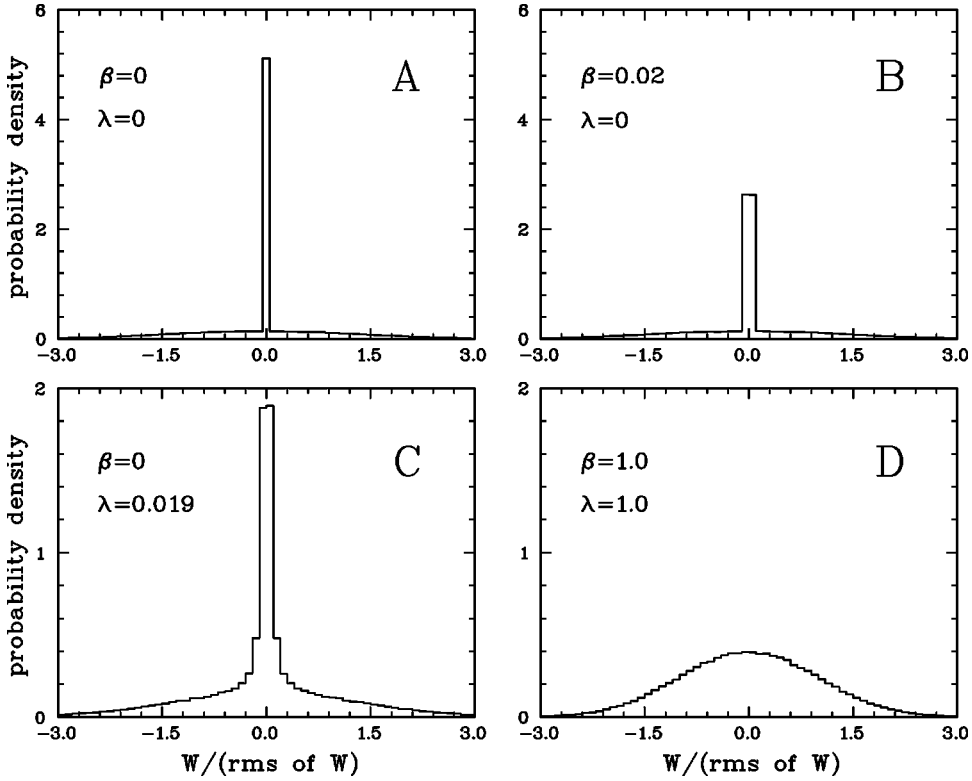

FIG. 2. Numerically generated distributions of transition matrix elements W_{if} for four different pairs of mixing parameters β and λ. The matrix elements are normalized to their root-mean-square value. The binning of the data is the same in the four parts of the figure. The scale of the ordinate is different in the upper and lower parts.

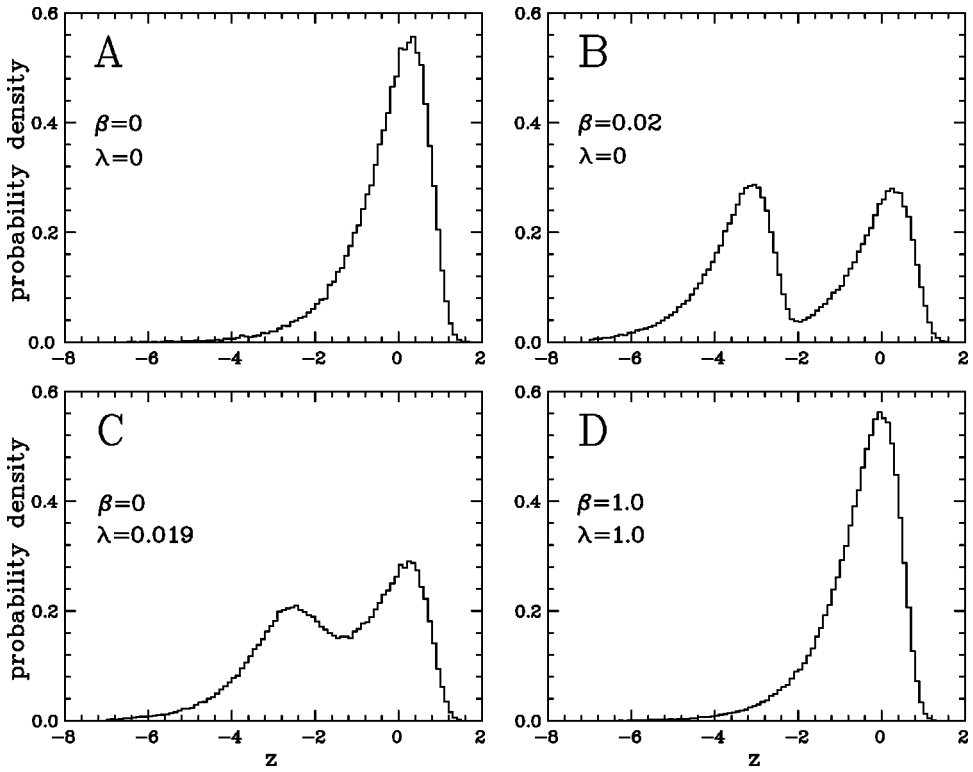

FIG. 3. Distributions of numerical transition probabilities B_{if}. These are the same data as in Fig. 2, but are reparametrized in terms of the variable z of Eq. (6).

cannot be distinguished from the case of complete symmetry breaking [Fig. 3(D)]. This occurs because $z \to -\infty$ when $W \to 0$; hence, the matrix elements with the value $W=0$ are found nowhere on the z axis.

In Sec. II it has been described how the secular variations of the statistical properties of the experimental data of Ref. [9] have been removed by help of the local average in Eq. (3). We have applied the same procedure to some of the present numerically generated data sets. Introducing a local average $\langle B_{if} \rangle$ instead of the global average $\overline{W_{if}^2} = \overline{B_{if}}$ used in Figs. 2 and 3 does not change the present results, i.e., along the spectrum of eigenstates there are no secular variations of the statistical properties of the eigenfunctions.

The numerical simulations clearly demonstrate that there indeed is an effect of symmetry breaking on the distributions. Hence, it is shown that the complexity of the wave functions alone is not enough to ensure Gaussian distributions of wave function, width, and transition amplitudes, as a naive application of the central limit theorem would imply.

V. QUALITATIVE EVALUATION OF THE RANDOM MATRIX MODEL WITH BROKEN SYMMETRY

In the present section we discuss the random matrix model in a heuristic fashion. This is an extension of the Sec. III to the case of broken symmetry. Although we believe that the model of Eqs. (23) and (28) can be completely solved analytically, we refrain from tackling that task. As we shall see, qualitative reasoning will provide sufficient understanding of the statistical behavior of the observables. Thus, our analytical derivations will be approximate and only exact in some limiting cases. Of course, we shall compare our approximate results with the above numerical simulations of the full model.

To obtain the distribution $P(W)$ we use the ansatz (28) for the transition operator and we need an ansatz for the distributions of the wave functions. The latter ones—in our model of the eigenvector components—are the entries of the orthogonal matrix U which diagonalizes the Hamiltonian,

$$U = \begin{bmatrix} U(0) & U(01) \\ U(10) & U(1) \end{bmatrix}, \tag{36}$$

where the matrices $U(j)$, $j=0,1$ are $N_j \times N_j$ orthogonal and $U(01)$ and $U(10)$ are $N_0 \times N_1$ and $N_1 \times N_0$ matrices, respectively, with the condition that the total U is orthogonal. Motivated by the numerical simulations in the previous section and by the general experience with wave-function distributions, we assume that the distributions of the entries can be approximated by Gaussians. More precisely, we estimate that the distributions of the $U(j)$ matrix elements are roughly given by $G(a, \kappa_j N^{-1/2})$, $j=0,1$, while those of the $U(01)$ and $U(10)$ matrix elements are roughly given by $G(a, \eta N^{-1/2})$. Thus, we reduce the problem to the determination of the three parameters κ_0, κ_1, and η. It is reasonable to assume that the former two are functions of the latter one, i.e., we set $\kappa_j = \kappa_j(\eta)$. This is motivated by the fact that η can replace the mixing parameter α (or λ) and that, apart from the level numbers N_0, N_1, the distribution of the elements of U is a function of the symmetry breaking. The final task is then to find the relation between the purely phenomenological parameter η and the parameter α which measures the root-mean-square symmetry-breaking matrix element and thus has a direct physical interpretation. In other words, we eventually have to specify the function $\eta = \eta(\alpha)$.

To construct a consistent guess for the functions $\kappa_j = \kappa_j(\eta)$, we notice that, in line with our basic assumptions, the combined distribution for the matrix elements of the total U reads

$$P_{N_0N_1}(a,\eta)=g_0^2G\left(a,\frac{\kappa_0(\eta)}{\sqrt{N}}\right)+g_1^2G\left(a,\frac{\kappa_1(\eta)}{\sqrt{N}}\right)$$
$$+2g_0g_1G\left(a,\frac{\eta}{\sqrt{N}}\right). \quad (37)$$

This form is consistent with the exact results (25) for arbitrary N_0 and N_1 and (27) for $N_0=N_1$. We mention in passing that we always deal with Gaussian approximations of distributions which, in some limiting cases, are for finite level number given by Eq. (11).

Let us consider the case $\alpha=0$ which yields the distribution (25). Comparison with Eq. (37) shows that

$$\eta^2(0)=0 \quad (38)$$

and

$$\kappa_j^2(0)=1/g_j, \quad j=0,1. \quad (39)$$

In the case of $\alpha=1$ and $N_0=N_1$, the exact result (27) leads to

$$\eta^2(1)=1 \quad (40)$$

and

$$\kappa_j^2(1)=1, \quad j=0,1. \quad (41)$$

Moreover, the functions $\kappa_j=\kappa_j(\eta)$ ought to be even in η. This suggests the ansatz

$$\kappa_j^2(\eta)=\frac{1}{g_j}+\left(1-\frac{1}{g_j}\right)\eta^2, \quad j=0,1. \quad (42)$$

It is reassuring that similar combinations of parameters do also show up in exact calculations of the spectral correlators.

A reasonable form for the function $\eta=\eta(\alpha)$ remains to be given. The function will parametrically depend on g_0 and g_1. We construct it by comparing the ansatz (37) with the distribution of the coefficients u_{im} of the eigenfunctions u_i from the numerical simulation of Sec. IV B. For each value of $\lambda=\alpha/D$, the optimum η was determined by maximizing the entropy (34). We have not attempted to assign errors to the values of η thus found. Instead we have convinced ourselves by inspection that the ansatz (37) reproduces the numerical distribution reasonably well. A typical example is given by Fig. 4. In this way the function $\eta=\eta(\alpha)$ was generated numerically. For the case of $N_0=N_1$ it is displayed in Fig. 5 together with the analytical expression

$$\eta^2(\alpha)=1-\exp(-\alpha/0.157) \quad (43)$$

that well approximates it. The numerical constant in the exponential is here equal to the level distance of Eq. (32). We emphasize, however, that the relation (43) is purely phenomenological. In Sec. VI we shall see that Eq. (43) can successfully be applied to the case of ^{26}Al, where D is different from Eq. (32), see Eq. (78) below, but the difference is not too large. Thus it seems that the numerical constant is indeed related to the level distance. This quantity shows a significant N dependence, see Eq. (31). It is at this point where the

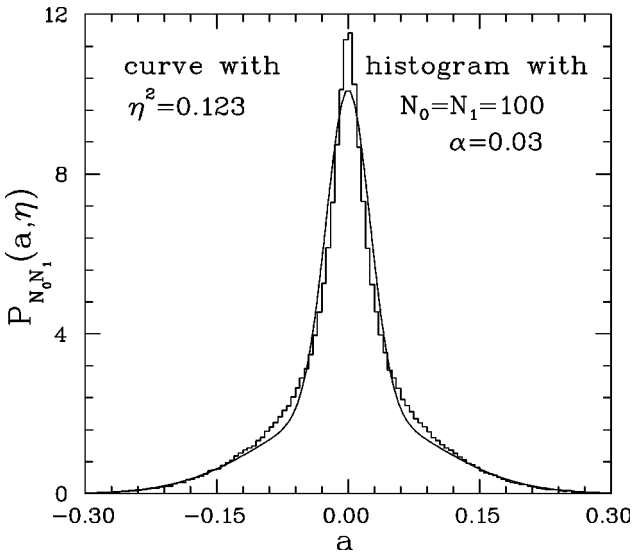

FIG. 4. The distribution of the components a of the eigenfunctions of H. The parameters of the numerical simulation are given on the figure. This yields the histogram. The curve is the function (37) with the optimum η.

premises of the central limit theorem are violated for the calculations of the distributions of the transition matrix elements. They cannot be a single Gaussian for all values of the parameters.

Having fixed all parameters in our qualitative model for the distribution of the eigenvector components, we can now calculate the distributions for the transition matrix elements $W_{if}=u_f^T\mathcal{O}u_i$. We emphasize that this involves, apart from the large N limit, no further approximation. We consider $i\neq f$, such that the initial and final states u_i and u_f are always different columns of the matrix U in Eq. (36). Due to isospin breaking, we have to distinguish four structurally different possibilities: in Case (M00) both u_i and u_f are among the first N_0 columns. We write

$$\text{Case } (M00):\ u_i=\begin{bmatrix}u_i(0)\\u_i(10)\end{bmatrix} \quad \text{and} \quad u_f=\begin{bmatrix}u_f(0)\\u_f(10)\end{bmatrix}.$$

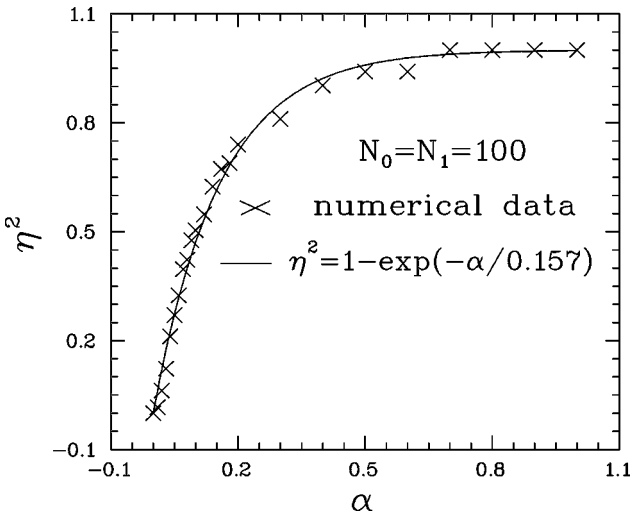

FIG. 5. The relation between α and η^2 for $N_0=N_1$. The crosses are from the numerical simulation. The curve is a phenomenological representation of the numerical results.

In Case ($M11$), both are from the last N_1 columns,

$$\text{Case } (M11): \quad u_i = \begin{bmatrix} u_i(01) \\ u_i(1) \end{bmatrix} \quad \text{and} \quad u_f = \begin{bmatrix} u_f(01) \\ u_f(1) \end{bmatrix}.$$

In Cases ($M01$) and ($M10$) u_i and u_f are from different parts in U; we have

$$\text{Case } (M01): \quad u_i = \begin{bmatrix} u_i(0) \\ u_i(10) \end{bmatrix} \quad \text{and} \quad u_f = \begin{bmatrix} u_f(01) \\ u_f(1) \end{bmatrix}.$$

$$\text{Case } (M10): \quad u_i = \begin{bmatrix} u_i(01) \\ u_i(1) \end{bmatrix} \quad \text{and} \quad u_f = \begin{bmatrix} u_f(0) \\ u_f(10) \end{bmatrix}.$$

Thus, for the case (Mjj'), $j,j'=0,1$ we will obtain a distribution $P_{jj'}(W_{if})$. Because of the symmetries $\mathcal{O}^T=\mathcal{O}$ and $W_{fi}=W_{if}$, the Cases ($M01$) and ($M10$) must yield identical distributions.

We proceed by generalizing the evaluation of the integral (16) in Sec. III B. Again, the distribution

$$P_{jj'}(W_{if}) = \int d[u_i] P(u_i) \int d[u_f] P(u_f) \delta(W_{if} - u_f^T \mathcal{O} u_i) \tag{44}$$

is rewritten in the form

$$P_{jj'}(W_{if}) = \frac{1}{2\pi} \int_{-\infty}^{+\infty} dt \exp(itW_{if}) R_{jj'}(t,\mathcal{O}), \tag{45}$$

where the main difficulty is the calculation of the function

$$R_{jj'}(t,\mathcal{O}) = \int d[u_i] P(u_i) \int d[u_f] P(u_f) \exp(-itu_f^T \mathcal{O} u_i). \tag{46}$$

In Case ($M00$), the distributions of the eigenvectors are according to our ansatz

$$P(u_i) = \left(\sqrt{\frac{N}{2\pi\kappa_0^2}} \right)^{N_0} \exp\left(-\frac{N}{2\kappa_0^2} u_i^T(0) u_i(0) \right) \times \left(\sqrt{\frac{N}{2\pi\eta^2}} \right)^{N_1} \exp\left(-\frac{N}{2\eta^2} u_i^T(10) u_i(10) \right) \tag{47}$$

for the initial state and

$$P(u_f) = \left(\sqrt{\frac{N}{2\pi\kappa_0^2}} \right)^{N_0} \exp\left(-\frac{N}{2\kappa_0^2} u_f^T(0) u_f(0) \right) \times \left(\sqrt{\frac{N}{2\pi\eta^2}} \right)^{N_1} \exp\left(-\frac{N}{2\eta^2} u_f^T(10) u_f(10) \right) \tag{48}$$

for the final state. Case ($M11$) is treated similarly. Case ($M01$) has a different structure: The initial-state distribution is as in Eq. (47), but the final-state distribution reads

$$P(u_f) = \left(\sqrt{\frac{N}{2\pi\eta^2}} \right)^{N_0} \exp\left(-\frac{N}{2\eta^2} u_f^T(01) u_f(01) \right) \times \left(\sqrt{\frac{N}{2\pi\kappa_1^2}} \right)^{N_1} \exp\left(-\frac{N}{2\kappa_1^2} u_f^T(1) u_f(1) \right). \tag{49}$$

However, one sees that in every case we may cast Eq. (46) into the form

$$\begin{aligned} R_{jj'}(t,\mathcal{O}) &= C_{jj'} \int d[u_i] \int d[u_f] \\ &\quad \times \exp\left(-\frac{N}{2} [u_i^T \; u_f^T] \mathcal{K}_{jj'} \begin{bmatrix} u_i \\ u_f \end{bmatrix} \right) \\ &= C'_{jj'} \det{}^{-1/2} \mathcal{K}_{jj'}. \end{aligned} \tag{50}$$

Here $C_{jj'}$ and $C'_{jj'}$ collect all normalization constants.

It is straightforward to write down the matrices $\mathcal{K}_{jj'}$. We define the diagonal matrices

$$D_0 = \operatorname{diag}\left(\frac{1}{\kappa_0^2} \mathbb{1}_{N_0}, \frac{1}{\eta^2} \mathbb{1}_{N_1} \right),$$

$$D_1 = \operatorname{diag}\left(\frac{1}{\eta^2} \mathbb{1}_{N_0}, \frac{1}{\kappa_1^2} \mathbb{1}_{N_1} \right), \tag{51}$$

and find

$$\mathcal{K}_{jj'} = \begin{bmatrix} D_j & it\mathcal{O}/N \\ it\mathcal{O}/N & D_{j'} \end{bmatrix} \tag{52}$$

in the four cases. An easy calculation yields

$$\begin{aligned} R_{jj'}(t,\mathcal{O}) &= \det{}^{-1/2} \left(\mathbb{1}_N + \frac{t^2}{N^2} D_j^{-1} \mathcal{O} D_{j'}^{-1} \mathcal{O} \right) \\ &= \exp\left[-\frac{1}{2} \operatorname{tr} \ln \left(\mathbb{1}_N + \frac{t^2}{N^2} D_j^{-1} \mathcal{O} D_{j'}^{-1} \mathcal{O} \right) \right] \end{aligned} \tag{53}$$

which leads in the large N limit to

$$R_{jj'}(t,\mathcal{O}) = \exp\left(-\frac{\overline{\mathcal{O}_{jj'}^2}}{2} t^2 \right). \tag{54}$$

The effective second moment $\overline{\mathcal{O}_{jj'}^2}$ of the operator $\mathcal{O}$ is defined by

$$\overline{\mathcal{O}_{jj'}^2} = \frac{1}{N^2} \operatorname{tr} D_j^{-1} \mathcal{O} D_{j'}^{-1} \mathcal{O}. \tag{55}$$

Hence, by performing the Fourier transform in Eq. (45), we arrive at

$$P_{jj'}(W_{if}) = G(W_{if}, \overline{\mathcal{O}_{jj'}^2}^{1/2}), \tag{56}$$

i.e., at a Gaussian in all four cases. The Gaussian form does not come as a surprise. The crucial and nontrivial result of this calculation is the explicit form of the effective second moments (55). Denoting the second moments of the blocks in the operator (28) by

$$\overline{\mathcal{O}^2(j)} = \frac{1}{N^2}\,\mathrm{tr}\,\mathcal{O}^2(j), \quad j=0,1,$$
$$\overline{\mathcal{O}_C^T\mathcal{O}_C} = \frac{1}{N^2}\,\mathrm{tr}\,\mathcal{O}_C^T\mathcal{O}_C, \tag{57}$$

we find after a simple computation in the four cases

$$\begin{aligned}
\overline{\mathcal{O}_{00}^2} &= \kappa_0^4\beta_I^2\overline{\mathcal{O}^2(0)} + \eta^4\beta_I^2\overline{\mathcal{O}^2(1)} + 2\kappa_0^2\eta^2\beta_C^2\overline{\mathcal{O}_C^T\mathcal{O}_C},\\
\overline{\mathcal{O}_{11}^2} &= \eta^4\beta_I^2\overline{\mathcal{O}^2(0)} + \kappa_1^4\beta_I^2\overline{\mathcal{O}^2(1)} + 2\kappa_1^2\eta^2\beta_C^2\overline{\mathcal{O}_C^T\mathcal{O}_C},\\
\overline{\mathcal{O}_{01}^2} &= \kappa_0^2\eta^2\beta_I^2\overline{\mathcal{O}^2(0)} + \kappa_1^2\eta^2\beta_I^2\overline{\mathcal{O}^2(1)}\\
&\quad + (\kappa_0^2\kappa_1^2+\eta^4)\beta_C^2\overline{\mathcal{O}_C^T\mathcal{O}_C},\\
\overline{\mathcal{O}_{10}^2} &= \overline{\mathcal{O}_{01}^2}.
\end{aligned} \tag{58}$$

The distributions $P_{jj'}(W_{if})$ of Eq. (56) describe Cases (Mjj'). These were defined by assuming that the structure of the initial and final states, i.e., their place of origin in the matrix (36) is known. In a set of experimental data, this information is usually lacking. Thus, the full distribution must be a proper superposition of the functions $P_{jj'}(W_{if})$. The weights in this superposition can be easily constructed: In Case $(M00)$, there are N_0 states and therefore $N_0(N_0-1)$ transitions. We recall that we exclude recoupling transitions with $i=f$. Since, altogether, there are N states and $N(N-1)$ transitions, the weight of Case $(M00)$ is $N_0(N_0-1)/N(N-1)$, which yields g_0^2 for large level numbers. In Case $(M11)$, one obviously finds g_1^2. Similarly, we find $N_0N_1/N(N-1)$, i.e., g_0g_1 for large level numbers, in both of Cases $(M01)$ and $(M10)$. Thus, collecting everything we eventually end up with

$$\begin{aligned}
P(W_{if}) &= g_0^2 G(W_{if}, \overline{\mathcal{O}_{00}^2}^{1/2}) + g_1^2 G(W_{if}, \overline{\mathcal{O}_{11}^2}^{1/2})\\
&\quad + 2g_0g_1 G(W_{if}, \overline{\mathcal{O}_{01}^2}^{1/2}),
\end{aligned} \tag{59}$$

where the individual variances are explicitly given in Eq. (58).

The choice of the transition operator $\mathcal{O}$ in Sec. IV B implies that the second moments of the blocks in Eq. (28) are (for large N_j)

$$\overline{\mathcal{O}^2(j)} = N_j^2/N^2 = g_j^2, \quad j=0,1 \tag{60}$$

and

$$\overline{\mathcal{O}_C^T\mathcal{O}_C} = \frac{N_0N_1}{N^2} = g_0g_1. \tag{61}$$

Inserting this and the definition (42) of the functions $\kappa_j(\eta)$ into (58) leads to

$$\begin{aligned}
\overline{\mathcal{O}_{00}^2} &= [(1-g_1\eta^2)^2 + \eta^4 g_1^2]\beta_I^2 + 2\eta^2(1-g_1\eta^2)g_1\beta_C^2,\\
\overline{\mathcal{O}_{11}^2} &= [(1-g_0\eta^2)^2 + \eta^4 g_0^2]\beta_I^2 + 2\eta^2(1-g_0\eta^2)g_0\beta_C^2,\\
\overline{\mathcal{O}_{01}^2} &= (1-2g_0g_1\eta^2)\eta^2\beta_I^2 + (1-\eta^2+2g_0g_1\eta^4)\beta_C^2.
\end{aligned} \tag{62}$$

Let us specialize these results to the case of the numerical simulation in Sec. IV B and see whether both are in qualitative agreement.

The numerical simulation has been performed with $N_0 = N_1$, whence

$$g_0 = g_1 = \frac{1}{2}. \tag{63}$$

Since the total strength of the operator $\mathcal{O}$ is immaterial, see the discussion of Eq. (29), one can set $\beta_I = 1$ which makes $\beta_C = \beta$. All this turns Eqs. (62) into the more transparent expressions

$$\begin{aligned}
\overline{\mathcal{O}_{00}^2} &= 1 - \left(\eta^2 - \frac{1}{2}\eta^4\right)(1-\beta^2),\\
\overline{\mathcal{O}_{11}^2} &= \overline{\mathcal{O}_{00}^2},\\
\overline{\mathcal{O}_{01}^2} &= 1 - \left(1-\eta^2+\frac{1}{2}\eta^4\right)(1-\beta^2),\\
\overline{\mathcal{O}_{10}^2} &= \overline{\mathcal{O}_{01}^2}.
\end{aligned} \tag{64}$$

If $\beta = 1$, the operator (28) completely mixes configurations with different isospin. In this case, Eqs. (64) yield

$$\overline{\mathcal{O}_{00}^2} = \overline{\mathcal{O}_{11}^2} = \overline{\mathcal{O}_{01}^2} = \overline{\mathcal{O}_{10}^2} = 1. \tag{65}$$

The distribution (59) of W_{if} then becomes

$$P(W_{if}) = G(W_{if}, 1), \tag{66}$$

i.e., a Gaussian for all η and, hence, for all α. This qualitatively agrees with the results of the numerical simulation, see Table I.

If $\alpha = 1$ (and $N_0 = N_1$), the Hamiltonian (23) is a full GOE matrix and its eigenstates have no isospin symmetry. According to Eq. (40), one then has $\eta^2 = 1$, Eqs. (64) yield

$$\overline{\mathcal{O}_{00}^2} = \overline{\mathcal{O}_{11}^2} = \overline{\mathcal{O}_{01}^2} = \overline{\mathcal{O}_{10}^2} = \frac{1}{2}(1+\beta^2), \tag{67}$$

and the distribution (59) becomes

$$P(W_{if}) = G\left(W_{if}, \left[\frac{1}{2}(1+\beta^2)\right]^{1/2}\right), \tag{68}$$

i.e., a Gaussian for all β. Again this qualitatively agrees with the results of the numerical simulation, see Table I.

If neither the Hamiltonian (23) nor the operator (28) mixes isospin, i.e., if β and η are zero, Eqs. (64) give

$$\overline{\mathcal{O}_{00}^2} = \overline{\mathcal{O}_{11}^2} = 1,$$

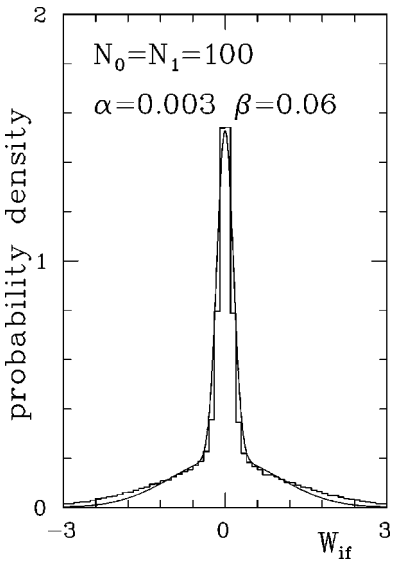

FIG. 6. A distribution of the transition matrix elements W_{if}. The histogram is due to the numerical simulation described in Sec. IV B. The curve is the qualitative model (59) with the parameters (71).

$$\overline{\mathcal{O}_{01}^2}=\overline{\mathcal{O}_{10}^2}=0. \tag{69}$$

In this limit, the distribution (63) takes the form

$$P(W_{if})=\frac{1}{2}[G(W_{if},1)+\delta(W_{if})]. \tag{70}$$

This says that half of the transition matrix elements is zero, namely the ones where i and f have different isospin. The other half is Gaussian distributed. This result is expected and agrees with the numerical simulation, see Table I and Fig. 2(a).

In Fig. 6 the distribution of W_{if} is displayed for the mixing parameters $\alpha=0.003$ and $\beta=0.06$. The histogram is the result of the numerical simulation in Sec. IV B. The curve is the qualitative model (59). The parameters follow from Eq. (43) which yields $\eta^2=0.0189$ and from Eqs. (64) which give

$$\begin{aligned}\overline{\mathcal{O}_{00}^2}&=\overline{\mathcal{O}_{11}^2}=0.981,\\ \overline{\mathcal{O}_{01}^2}&=\overline{\mathcal{O}_{10}^2}=0.0223.\end{aligned} \tag{71}$$

This illustrates that the qualitative model reproduces the essential features of the numerical data although it does not describe them quantitatively.

VI. INTERPRETATION OF THE EXPERIMENTAL DATA

In Sec.VI A, the experimental data described in Sec. II are compared to the prediction of the qualitative solution (58) of the model of Sec. IV A. In Sec. VI B, we discuss the effect that symmetries other than isospin have on the data. Parity conservation is used as an example.

A. Isospin breaking in ^{26}Al

The results of Secs. IV and V suggest that the distribution of the reduced electromagnetic transition probabilities, displayed in Fig. 1, does carry a signature of isospin breaking. In order to verify this, we compare in the present section the random matrix model to the experimental data.

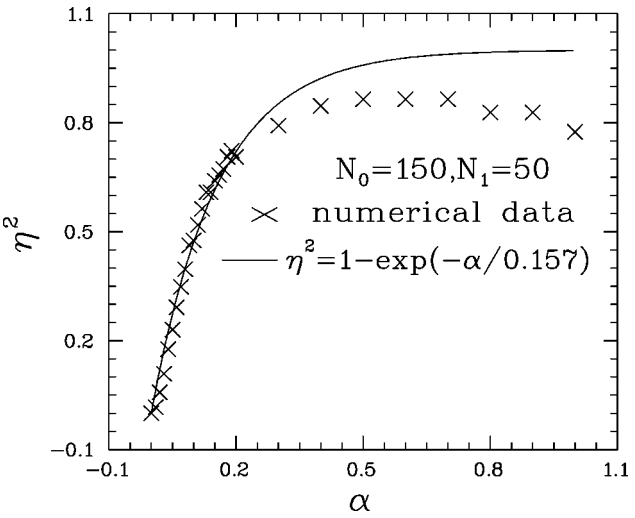

FIG. 7. The relation between α and η^2 for $N_0\neq N_1$.

The parameters of the random matrix model are chosen as follows. The dimensions N_0, N_1 of the blocks in the Hamiltonian (23) are not equal. Rather one has

$$N_0/N_1=3 \tag{72}$$

which approximately corresponds to the ratio of the densities of states with $T=0$ and $T=1$ in ^{26}Al. This entails

$$g_0=\frac{3}{4},\quad g_1=\frac{1}{4}. \tag{73}$$

The parameter which quantifies isospin breaking in the Hamiltonian was set to $\alpha=0.028$. This value has been taken from the analysis of the eigenvalue statistics in Ref. [5]. We must convert it to the parameter η of the qualitative model of Sec. V. However, so far it is not clear whether Eq. (43) applies because that function is based on a numerical simulation with $N_0=N_1$ which is different from (72). We have therefore performed another numerical simulation of the distribution of the eigenvector coefficients a. This simulation was done with $N_0=150$ and $N_1=50$. For each α, the function (37) was again compared to the numerical distribution of a and the optimum η was determined. This yielded the crosses on Fig. 7. It turns out that the function (43) again reproduces the numerical data if one considers only the range of $\lambda=\alpha/D\lesssim 1$. Note that in the case at hand, the level distance is

$$D=0.192. \tag{74}$$

For $\lambda=\alpha/D>1$ the function (43) does not reproduce the data of Fig. 7 because the Hamiltonian (23) does not become a GOE matrix for any value of α if $N_0\neq N_1$. Due to Eq. (74) the numerical constant in Eq. (43) is no longer equal to the level distance.

One finds

$$\eta^2=0.163 \tag{75}$$

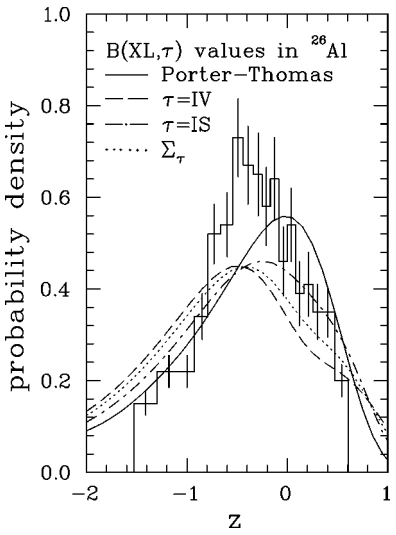

FIG. 8. The distribution of reduced transition probabilities in ^{26}Al. The experimental histogram is the same as in Fig. 1. The full curve is the Porter-Thomas distribution (9). The remaining curves have been obtained with the qualitative model (59). The dashed curve—labeled $\tau=$IV—has been obtained with the isovector transition operator; the dot-dashed curve—labeled $\tau=$IS—is from the isoscalar transition operator; the dotted curve—labeled Σ_τ—is the weighted sum of both.

for the present case of ^{26}Al.

Due to the fact that ^{26}Al is a mirror nucleus, i.e., it has the isospin projection $T_z=0$, the transition operator is uniquely determined by its isospin structure.

If $\mathcal{O}$ is isoscalar it can by definition not connect states with different isospin. The parameter β_C in Eq. (28) is then zero and, of course, $\beta=0$. If the operator is isovectorial it cannot connect states with the same isospin. This is obvious for states having $T=0$. For states having $T=1$, this follows from the symmetry properties of $\mathcal{O}$ in isospin space. See Chap. 9 of Ref. [16], especially the discussion following Eq. (9.107). The parameter β_I in Eq. (28) is then zero. We evaluate the distribution (59) for these two cases.

Let the operator $\mathcal{O}$ be isoscalar, whence $\beta_C=0$. We set $\beta_I=1$, make use of Eqs. (77) and (79), and obtain from Eqs. (62)

$$\overline{\mathcal{O}^2_{00}}=0.922,$$
$$\overline{\mathcal{O}^2_{11}}=0.785, \tag{76}$$
$$\overline{\mathcal{O}^2_{01}}=\overline{\mathcal{O}^2_{10}}=0.153.$$

This gives the distribution (59) of the isoscalar matrix elements W_{if}. It is transformed to the variable

$$z=\log_{10}\frac{W^2_{if}}{\overline{W^2_{if}}}. \tag{77}$$

The result is the dot-dashed curve on Fig. 8.

Now let the operator $\mathcal{O}$ be isovectorial, whence $\beta_I=0$. We choose $\beta_C=1$, use Eqs. (75) and (73), and obtain from Eq. (62)

$$\overline{\mathcal{O}^2_{00}}=0.0782,$$
$$\overline{\mathcal{O}^2_{11}}=0.235, \tag{78}$$
$$\overline{\mathcal{O}^2_{01}}=0.847.$$

This gives the distribution (59) of the isovectorial matrix elements W_{if}. Again this distribution is transformed to the variable (77). The result is the dashed curve on Fig. 8.

One sees that both the distribution with $\tau=$IV and the one with $\tau=$IS are shifted with respect to the Porter-Thomas distribution (9). This is a consequence of the appearance of Gaussian distributions with different widths in Eq. (59). The shoulder on the right-hand side of the isovector distribution in Fig. 8 even hints to the appearance of two peaks as in the numerical simulations in Figs. 3(b) and 3(c). However, in ^{26}Al, isospin mixing is too large (namely, $\lambda=0.146$) as to let the peaks separate. Remember that it is the class of small matrix elements that produces the peak which is centered at negative values of z. The class of large matrix elements leads to a peak which is centered close to $z=0$. The smaller the relative strength of the small matrix elements is, the more clearly the peaks separate.

There is a factor other than α (or η^2) which determines the shape of the distributions on Fig. 8. For the isoscalar problem the class of the large matrix elements is the one with variance $\overline{O^2_{00}}$, see Eqs. (76). It has the largest weight in the distribution, namely g_0^2, see Eqs. (59) and (73). Therefore the distribution is shifted only slightly to negative values of z. For the isovector problem the class of the small matrix elements is the one with variance $\overline{O^2_{00}}$, see Eqs. (78), which has the largest weight. Therefore the distribution is shifted more strongly to negative values of z. This makes the isovector matrix elements more sensitive to isospin breaking than the isoscalar matrix elements.

The distributions for the isovector and isoscalar cases have been summed with the weights 530 and 343, respectively. These are the numbers of observed transitions, see Ref. [9]. The result is the dotted curve on Fig. 8. It is shifted with respect to the Porter-Thomas distribution by about the same amount as the experimental data. However, the data are more strongly peaked around $z\approx-0.5$ than the present theory. This discrepancy must be attributed, at least partially, to the way the detection thresholds have been taken into account, see Eq. (10): The percentage of undetected transitions may have been underestimated because its estimation was based on the Porter-Thomas distribution. The distributions that include isospin violation predict a larger probability of events outside the range of the experimental data than does the Porter-Thomas distribution.

We conclude that the present investigation supports the conjecture of Ref. [9] which attributes the discrepancy between the Porter-Thomas distribution and the experiment to partial isospin breaking in ^{26}Al.

B. Other symmetries of the system: parity

The nucleus ^{26}Al has more than only isospin symmetry. Especially there are quantum numbers that are exactly conserved or nearly so. For definiteness let us discuss parity

conservation. Should it be included into all the above considerations that have focused on isospin conservation alone?

The matrix model of Sec. IV A can be extended to take parity into account. If the system has two possible values of isospin $T=0,1$ (isospin being broken to some extent) and parity $\pi=\pm 1$ (parity being a very well conserved symmetry), the Hamiltonian H as well as the operator $\mathcal{O}$ can be written in the following block form:

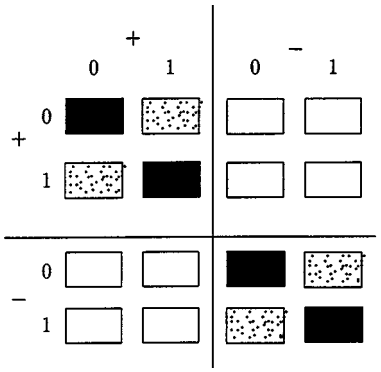

(79)

The four larger blocks are related to parity symmetry: The two blocks on the diagonal correspond to transitions between positive- and negative-parity configurations, respectively. The off-diagonal blocks correspond to parity-violating transitions. They are zero in the present context.

Each of the larger blocks is broken down into four smaller blocks related to isospin symmetry. They correspond, in an obvious way, to isospin conserving and isospin violating transitions.

The ''color'' of the blocks schematically shows the strength of the matrix elements. The black blocks contain large matrix elements, allowed by both isospin and parity conservation. The dotted blocks contain small matrix elements, allowed by parity conservation but forbidden by isospin conservation. The white blocks contain zero matrix elements, forbidden by parity conservation.

Since in the present context parity is considered an exact symmetry, the experimenters do not try to measure parity-violating transitions. They assume them to be zero and—this is the important point—they do not even list them on their records. Hence, the experimental data set consists of the matrix elements in the two larger diagonal blocks. They are thus equivalent to the data that we have assumed in all foregoing considerations.

Hence, the existence of exactly conserved quantities in addition to the partially conserved isospin quantum number is irrelevant if they are not measured. The existence of partially conserved quantum numbers other than isospin would, however, alter the above results.

VII. SUMMARY AND CONCLUSION

In the present study the effect of a partially broken symmetry has been investigated for the distributions of wave-function components and transition probabilities. This has been done by means of a random matrix model similar to the one introduced by Rosenzweig and Porter [3]. However, in the present model not only the Hamiltonian but also the transition operator may break the symmetry. This was dictated by the experimental material at hand and the symmetry that we had in mind. The data consist of a set of reduced electromagnetic transition probabilities in the nucleus ^{26}Al. The symmetry is isospin conservation. Eletromagnetic transition operators are in general not isospin conserving.

A numerical simulation has shown that neither the components of the eigenfunctions nor the transition matrix elements follow Gaussian distributions. This is counterintuitive since the central limit theorem seems to require Gaussian distributions if the wave functions are ''sufficiently complicated.'' Instead, the numerical simulation suggests that the ensembles of both, the components of the eigenfunctions and the transition matrix elements, comprise at least one class of small elements and one class of large elements. The physical origin of these classes is clear: The small elements are isospin violating; the large elements are isospin allowed. At best, each of the classes has a Gaussian distribution. The probability density of the whole ensemble is then a superposition of Gaussians with different parameters.

This idea has been worked out in detail and results in a qualitative analytical evaluation of the random matrix model. It yields simple formulas for the parameters of the Gaussians. Its practical use is to circumvent easily the demanding numerical simulations. Conceptually, it offers to see in detail why the premises of the central limit theorem are not given: the elements in the different classes depend in different ways on the symmetry-breaking parameter α as well as the dimension N of the space. It is well known that in the limit of $N\rightarrow\infty$ an ever smaller value of α suffices to make the above classes indistinguishable and thus to produce simple Gaussian distributions of the eigenvector components and the transition matrix elements. However, this is what happens if N is taken to infinity such that the parameter $\lambda=\alpha/D$ goes to infinity. If N is finite or if it is taken to infinity together with $\alpha\rightarrow 0$ such that λ remains finite, then the above mentioned classes conserve their identity. It is this situation which the present paper deals with.

The present results thus support a conjecture formulated in Ref. [9] on the basis of the data collected from ^{26}Al: The authors conjectured that the distribution of the electromagnetic transition probabilities carries the signature of partial isospin breaking. The present theory offers a qualitative understanding of the data. Whether it can quantitatively reproduce the data remains to be seen. We have not attempted to fit the theory to the data.

A caveat seems necessary: The random matrix model (23) applies to any partially broken quantum number—it is not specific for isospin. Certainly, the available information on isospin breaking in ^{26}Al requires that the distribution of the transition probabilities differs from a Porter-Thomas distribution to the extent given by the dotted curve on Fig. 8—but the data may in principle and in addition carry the signature of other partially conserved quantum numbers. These may not be as fundamental as isospin but rather given by the specific form of the effective nucleon-nucleon interaction in the sd shell.

Very recently, an analytical calculation, based on the supersymmetry method, of the wave-function statistics in coupled chaotic systems was presented in Ref. [17]. These results are valid for the case of broken time-reversal invariance and therefore, unfortunately, are not applicable to the

case of conserved time-reversal invariance which is discussed in the present paper.

ACKNOWLEDGMENTS

We thank H. A. Weidenmüller, A. Richter, and V. K. B. Kota for fruitful discussions. We are indebted to G. E. Mitchell and J. F. Shriner, Jr. for supplying the experimental data of ^{26}Al and for suggestions and criticisms during the work. C.I.B. acknowledges the financial support granted by the Fritz Thyssen Stiftung, Deutsche Akademische Austauschdienst (DAAD), and Conselho Nacional de Desenvolvimento e Pesquisa (CNPq) at different periods during this work. T.G. acknowledges support from the Heisenberg Foundation.

[1] E.P. Wigner, in *Statistical Theories of Spectra: Fluctuations*, edited by C.E. Porter (Academic Press, New York, 1965), p. 199.
[2] T. Guhr, A. Müller-Groeling, and H.A. Weidenmüller, Phys. Rep. **299**, 189 (1998).
[3] N. Rosenzweig and C.E. Porter, Phys. Rev. **120**, 1698 (1960).
[4] G.E. Mitchell, E.G. Bilpuch, P.M. Endt, and J.F. Shriner, Jr., Phys. Rev. Lett. **61**, 1473 (1988).
[5] T. Guhr and H.A. Weidenmüller, Ann. Phys. (N.Y.) **199**, 412 (1990).
[6] D.M. Leitner, Phys. Rev. E **48**, 2536 (1993); D.M. Leitner, H. Köppel, and L.S. Cederbaum, Phys. Rev. Lett. **73**, 2970 (1994).
[7] C. Ellegaard, T. Guhr, K. Lindemann, J. Nygård, and M. Oxborrow, Phys. Rev. Lett. **77**, 4918 (1996).
[8] H. Alt, C.I. Barbosa, H.-D. Gräf, T. Guhr, H.L. Harney, R. Hofferbert, H. Rehfeld, and A. Richter, Phys. Rev. Lett. **81**, 4847 (1998).
[9] A.A. Adams, G.E. Mitchell, and J.F. Shriner, Jr., Phys. Lett. B **422**, 13 (1998).
[10] A. Andersen, C. Ellegaard, A.D. Jackson, and K. Schaadt (unpublished).
[11] A.A. Adams, G.E. Mitchell, W.E. Ormand, and J.F. Shriner, Jr., Phys. Lett. B **392**, 1 (1997).
[12] J.F. Shriner, Jr. (private communication).
[13] G. Auger, O. Bohigas, and J. Flores, Notas de Fisica **3**, 1 (1980).
[14] T.A. Brody, J. Flores, J.B. French, P.A. Mello, A. Pandey, and S.S.M. Wong, Rev. Mod. Phys. **53**, 385 (1981).
[15] Note that there is a lack of precision in the text of [8] below Eq. (1) there: The condition of equal dimensions of the GOE blocks is missing.
[16] P.J. Brussaard and P.W.M. Glaudemans, *Shell-Model Applications in Nuclear Spectroscopy* (North-Holland, Amsterdam, 1977).
[17] A. Tschersich and K.B. Efetov, e-print cond-mat/9911284.